Highly Conductive Tungsten Doped Tin(IV) Oxide Transparent Electrodes Delivered by Lattice-Strain Control

Sanjayan Sathasivam[a,b],* Sapna D Ponja[b], Seonghyeok Park[a], Clara Sanchez-Perez[b,c], Christopher Blackman[b], Ivan P Parkin[b] and Claire J Carmalt[b]*

*Corresponding authors

[a]School of Engineering, London South Bank University, London, SE1 0AA, UK

[b]Materials Chemistry Centre, Department of Chemistry, University College London, 20 Gordon Street, London WC1H 0AJ, UK

[c]Instituo de Energía Solar, Universidad Politécnica de Madrid, 28040 Madrid, Spain.

E-mail: s.sathasivam@lsbu.ac.uk & c.j.carmalt@ucl.ac.uk

Abstract

Alternatives to tin doped indium oxide transparent conductors are needed to meet the growing demand for modern electronic devices. Here, we present the first chemical vapour deposition route to tungsten doped SnO_2 thin films. Resistivities as low as 5.9 x 10^{-4} Ω.cm and electron mobilities as high as 30 cm^2 V^{-1} s^{-1} were achieved by substituting tungsten(V) for tin(IV) in the tin oxide lattice. Le Bail fitting of the XRD data showed that tungsten(V) causes minimal distortion to the SnO_2 unit cell due to its closely matched radius to tin(IV). Furthermore, crystallographic preferential orientation in the [200] that is thought to facilitate high mobility was also seen. X-ray photoelectron spectroscopy analysis suggests that W is present in the +5 state as opposed to +6 therefore minimising ionised impurity scattering hence also helping achieve the observed high electron mobilities. The tungsten doped films had optical band gaps of 3.7 eV thus enabling transparency to visible light.

Keywords: Transparent electrodes, metal oxides, doping, thin films, chemical vapor deposition, lattice strain

Introduction

Transparent conducting oxides (TCOs) are wide band gap (>3.1 eV) semiconductors with high optical transparency (>80%) to visible light and low electrical resistivity (<x10^{-3} Ω.cm) due to high carrier concentrations of 10^{20} cm^{-3}.[1–5] They have application as electrodes in many modern electronic devices including photovoltaics, touchscreens and displays.[6–8]Tin-doped In_2O_3 (ITO) dominates as the TCO of choice due to record-low resistivities in the 10^{-5} Ω.cm range. However, supply and cost issues related to indium have meant alternative TCOs need to be further developed as replacements to ITO.[1] Mo-doped In_2O_3 (IMO) is a well investigated TCO material that often displays superior optoelectronic properties to ITO but has had little commercial uptake.[9,10] In fact, recent work has shown that due the localized nature of the Mo(V) d-orbitals that lie high in the conduction band of In_2O_3, extremely high electron mobilities of ~150 $cm^2V^{-1}s^{-1}$ for IMO are achievable compared to ~80 $cm^2V^{-1}s^{-1}$ for ITO.[9] This highlights the point that by carefully selecting the dopant for TCO materials excellent optoelectronic results can be achieved.

A widely used alternative to ITO is F:SnO_2 (FTO).[11] It is relatively inexpensive, possesses a band gap of 3.6 eV and is inherently n-type with resistivities <4x10^{-4} Ω.cm commonly achieved.[12] However, interstitial F^- ions do also readily form leading to a smaller carrier concentration through self-compensation, lower electron mobility via increased scattering and therefore lower conductivity than what would otherwise be expected.[12]

Antimony is also an effective dopant for SnO_2 that yields resistivities as low as 5x10^{-4} Ω.cm. However, antimony's multi-valency and readiness to form charge compensating Sb^{3+} acceptor states such that scope for further decrease in resistivity is limited.[13,14] Recently, our computational and experimental studies have shown that tantalum is a near ideal dopant for SnO_2.[13] In Ta:SnO_2, formation of acceptor species, such as interstitial Ta and the clustering of substitutional Ta with oxygen vacancies that can reduce the carrier concentration through charge compensation, are thermodynamically unfavorable.[13] Furthermore, and similar to what is observed with the high mobility TCO Mo:In_2O_3, due to the lack of hybridization of the Ta 5*d* states with

the conduction band minima of SnO_2, the effective mass remains low leading to high electron mobilities in the Ta-doped films.[13] Furthermore, Ta favours the +5 oxidation state in SnO_2 therefore contributing one electron per Sn^{4+} substituted to reduce resistivity.

Tungsten is another transition metal that has been studied as a suitable dopant to enhance the conductivity of SnO_2.[15–18] Tungsten commonly occurs in the +4, +5 and +6 oxidation state. These W ions have similar radius to Sn^{4+}, therefore making them sufficiently soluble.[19] Ideally if W occupies the +5 oxidation state in SnO_2, and hence is a donor in the 1+ charge state, then carrier concentration can be enhanced for electrical conduction whilst ionized impurity scattering is minimized. Like Ta:SnO_2, where the Ta 5*d* states appear ~1.4 eV above the CBM of SnO_2, W 5*d* states are predicted to lie high in the SnO_2 conduction band and cause minimal disturbance to the CBM hence allowing for low effective electron mass, high mobilities and high conductivities according to recent computational studies.[13,20]

W:SnO_2 films have been grown previously using physical vapour deposition routes such as pulsed plasma deposition (PPD), pulsed laser deposition (PLD) and magnetron sputtering.[15–17] These films have resistivity values in the 10^{-3} Ω.cm range, however a resistivity of 3.5 x10^{-4} Ω.cm has been achieved using TiO_2 seed layers, primarily due to high electron mobilities facilitated by extreme crystallographic orientation in the [200].[18] Aside from PVD there are reports of sol-gel and chemical spray pyrolysis methods to W:SnO_2,[21,22] however a chemical vapour deposition (CVD) route - the technique of choice for commercial FTO films - for the fabrication of W:SnO_2 films is yet to be reported.

In this paper, we show the growth, characterization and optoelectronic testing, for the first time, of CVD produced W:SnO_2 films on glass substrates.[23–26] CVD is versatile fabrication technique with non-line of sight deposition capabilities.[27,28] It enables well adhered coatings at high growth rates under ambient pressure and is therefore used for the production of industrial TCOs.[27] The W:SnO_2 films produced by CVD as described in this paper, show a resistivity of 5.90 x 10^{-4} Ω.cm, the lowest reported to date for a W:SnO_2 film grown on glass. The electron mobilities of the films remained high (~30 cm^2 V^-

^{1} s^{-1}) despite the increasing W content. This is attributed to the promotion lack of hybridization of the W states with the SnO_2 CBM and helped by crystallographic preferred orientation in the [200].[13,20]

Experimental

Film synthesis

All precursors were purchased from Aldrich and used as received.

AACVD depositions were carried out on a custom built cold-wall reactor where a float glass (that has a ~50 nm amorphous SiO_2 layer to prevent the migration of ions into the film) was positioned on a graphite block containing a Watlow cartridge heater regulated by a Cr-Ni-Al (Type-K) thermocouple. A stainless-steel top plate was positioned 0.8 cm above the substrate to promote laminar flow. The W doped SnO_2 films were grown using an AACVD process using monobutyltin trichloride (MBTC) (0.3 mL, 1.77 mmol) and $W(CO)_6$ (0, 0.2, 0.5, 0.7 and 1 mol.%) dissolved in dry methanol (10 mL, 394 mmol) and two solutions were atomized using a Johnson Matthey Liquifog® piezoelectric ultrasonic humidifier with the tin precursor flow rate kept at 0.5 L min^{-1} using air (BOC, 99.99%). The glass substrate was maintained at 450 ^{o}C. At the end of the depositions for both systems, the reactor was turned off and cooled under a flow of nitrogen until 100 ^{o}C after which point the samples were removed. The coated substrates were handled and stored in air.

Instrumental conditions

X-ray diffraction (XRD) was carried out using a modified Bruker-Axs D8 diffractometer with parallel beam optics and a PSD LynxEye silicon strip detector with a monochromated Cu Kα source operated at 40 kV with 30 mA emission current. The incident beam angle was set at 0.5°, and the 2θ range of 10°−65° was measured with a step size of 0.05° at 1 s/step. Unit Cell parameters were determined by carrying out using Profex (v4.3.6) software by applying a Le Bail fit to the collected XRD patterns.[29] A JEOL JSM-6301F field emission SEM (5 kV accelerating voltage) was used for scanning electron microscopy (SEM) measurements. Samples were coated with gold to avoid charging. Energy dispersive X-ray spectroscopy (EDS) was measured using an

Oxford Instruments EDS system using accelerating voltage of 15 kV. Optical measurements were performed using a PerkinElmer Fourier transform Lambda 950 spectrometer over a wavelength range of 300−2500 nm. X-ray photoelectron spectroscopy (XPS) was performed by using a Thermo Scientific K_α photoelectron spectrometer using monochromatic Al Kα radiation. Higher resolution scans (400 µm diameter spot size) were recorded at a binding energy step size of 0.1 eV for the principal peaks of Sn(3d), W(4f) and C(1s) at a pass energy of 50 eV. The samples were charge compensated during measurement using argon ion and electron flood guns. The peaks were fitted by with CasaXPS software using a Gaussian-Lorentzian line shape and Shirley background subtraction on the raw spectral envelopes. The binding energies adjusted to adventitious carbon (284.5 eV) for charge correction (ESI Figure S1). Hall effect measurements were performed using the van Der Pauw method to determine the resistivity (ρ), free carrier concentration (n), and mobility (µ) using an Escopia HMS-3000 instrument with a 0.51 T magnet.

Results and Discussion

Nominally undoped and W: SnO_2 films were prepared from the AACVD reaction of monobutly tinchloride (MBTC), tungsten hexacarbonyl and methanol. Films were grown on glass substrates held at 450 ^oC with air as the carrier gas. All films were well adhered to the substrate, passing the Scotch tape test.[30] Energy dispersive X-ray spectroscopy (EDS) showed the bulk W concentration to be 0, 1, 1.5, 2 and 3 at.% from precursor solutions containing 0, 0.2, 0.5, 0.7 and 1 mol.% of $W(CO)_6$ relative to MBTC – indicating a liner increase in W concentration the SnO_2 films with increasing $W(CO)_6$ precursor and therefore operating under a mass transport limited growth regime (Figure 1).[31–33]

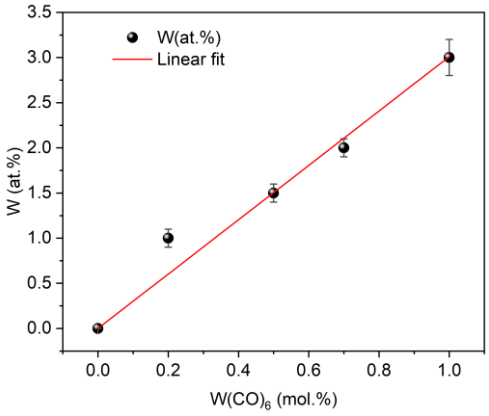

Figure 1: The linear relationship between the $W(CO)_6$ concentration in the methanol precursor solution and the atomic W concentration in the W:SnO_2 films.

X-ray diffraction (XRD) analysis showed only the tetragonal rutile phase of SnO_2 to be visible, suggesting solid solution formation through substitutional doping (Figure 2a). Substitutional doping can induce structural changes to the lattice by expanding or contracting the unit cell, depending on the difference in the radii of the host and dopant ions. W-ions in the 6 coordination have an ionic radius of 0.66 Å (W^{4+}), 0.62 Å (W^{5+}) or 0.60 Å (W^{6+}) which are similar to the ionic radius of 6 coordinate Sn(IV) of 0.69 Å.[34–36] As a result, minimal observable distortion was expected. Shifting of peaks caused by strain to the unit cell is more significant at higher 2θ angles. The (211) reflection at 51.7 ° was magnified (Figure 2b) to observe if such shifting was observable in the data for the W:SnO_2 films. A slight move towards higher 2θ values was apparent for only the 3 at.%. However, when quantified by applying a Le Bail fit to the XRD patterns to determine the unit cell parameters (Figure 2c & Table 1) no change beyond the standard deviation was observed in both the *a* and *c* lengths and thus the cell volume with W incorporation across all samples. It should be noted that the unit cell volumes of the SnO_2 and W:SnO_2 CVD films are ~0.4% larger than that determined for the reference pattern (i.e. SnO_2 calculated) due to their longer lengths along the *a* axis. This observation is likely caused due to the growth of the films on amorphous SiO_2 layer of the glass substrates and has been previously observed for metal oxide thin films.[37]

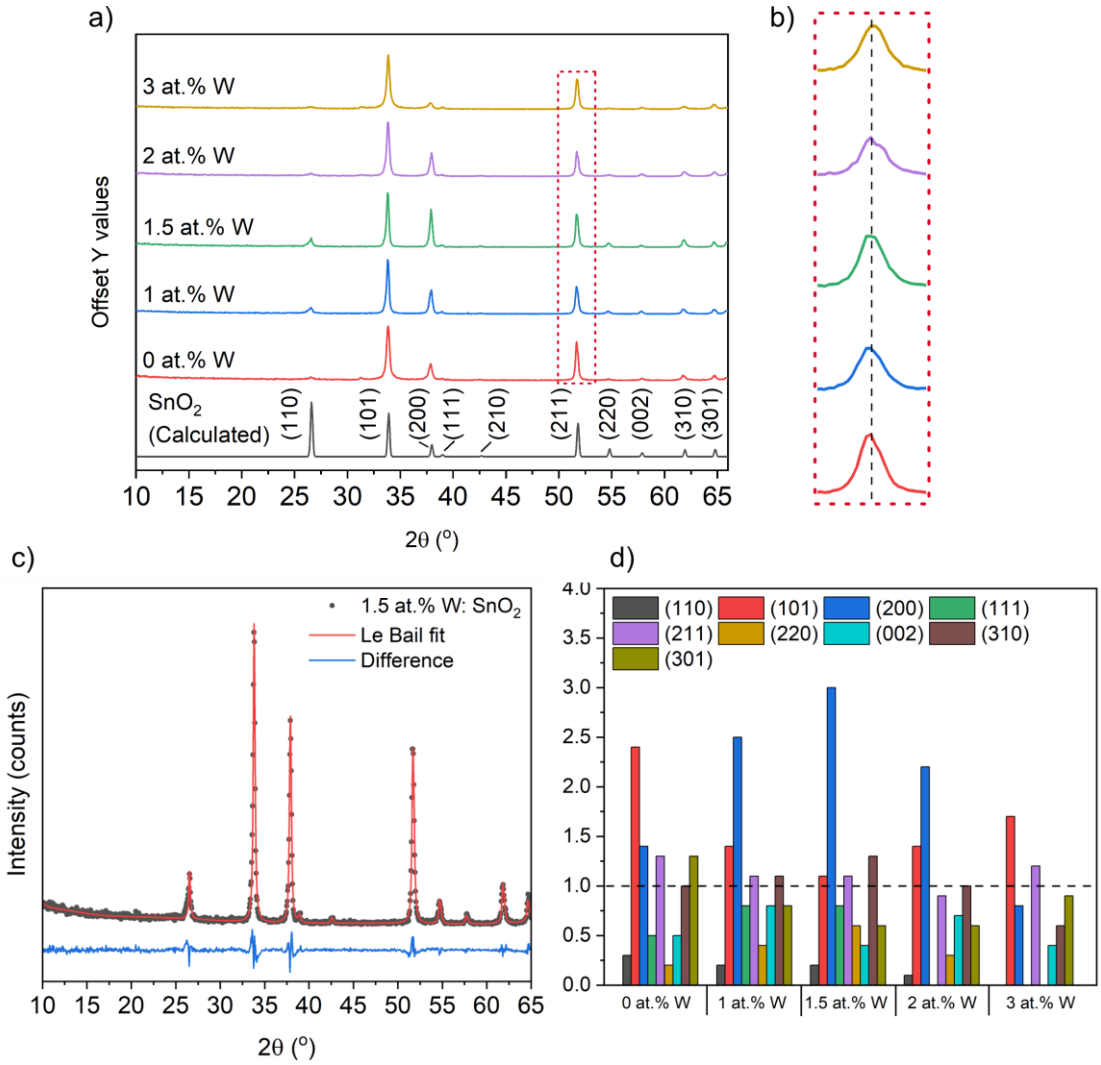

Figure 2: a) XRD patterns for the 0-3 at.% W doped SnO_2 films as well as the calculated pattern for SnO_2 in the cassiterite phase is also shown. b) a magnification of the (211) peaks showing no significant shifting after W substitution in SnO_2. c) The La Bail fit for the most conductive film (1.5 at.% doped W: SnO_2). d) The variation of texture coefficients across different W concentrations in the SnO_2 films where texture coefficient values above one indicates preferential growth for that plane.

Table 1: The unit cell parameters as determined via a Le Bail fit of the XRD patterns for the 0, 1, 1.5, 2 and 3 at.% W doped SnO_2 films grown by CVD on glass substrates. The values within paratheses indicate the error for that distance or volume.

W conc. / at.%	a/ Å	c/ Å	Volume / Å^3
0 (ref. pattern)	4.73800	3.18650	71.5326
0	4.7481(7)	3.1869(6)	71.847(17)
1	4.7452(6)	3.1899(5)	71.827(14)
1.5	4.7447(5)	3.1903(5)	71.821(14)

2	4.7451(6)	3.1900(5)	71.826(14)
3	4.7468(7)	3.1882(7)	71.837(19)

Preferential growth in polycrystalline films such as SnO_2 can be an important factor impacting the electronic properties, such as electron mobility and resistivity. Nakao et al produced highly (200) oriented W:SnO_2 films with the aid of an anatase TiO_2 seed layer, leading to high electron mobilities and low resistivities.[18] However, the W:SnO_2 films grown in our study using a CVD route on commercial float glass showed, without the need of any structure directing seed layer, the necessary (200) preference – helped by the W dopant (Figure 2c). Dopant induced preference for (200) has previously been observed by Kumar et al for chemical spray deposited W:SnO_2 gas sensing films.[22] They observed an increase in preference for the (200) peak upon W incorporation which then helped improve senor response towards NO_2 gas.[22] With respect to the enhancement of electrical properties, our CVD results show the merits of W as an ideal dopant for SnO_2. W is able to promote growth of the films with (200) preference (Figure 2c) - up to 3x increase (200) preference was observed in the W:SnO_2 films compared to the nominally undoped sample - whilst causing no observable distortion to the SnO_2 unit cell (Table 1).

X-ray photoelectron spectroscopy (XPS) was carried out on the surface (<10 nm) of the films to determine chemical state of Sn, O and W. The Sn 3d spectra showed no asymmetry and indicating the presence of only Sn(IV), corresponding to a Sn $3d_{5/2}$ binding energy of 486.3 eV (Figure 3a). The O 1s peaks (Figure 3b) however, showed asymmetry and revealed two environments matching O bound to W in the lattice ($O_{lattice}$) at 530.0 eV and a secondary, slightly broader O 1s peaks at 531.5 eV belonging to metal OH groups that are common on metal oxide surfaces.[38] As expected, no W 4f peaks were observed for the nominally undoped sample whilst only small bumps in the region were observed for the 1.0 and 1.5 at.% doped films. At the higher doping levels of 2 and 3 at.%, fitting of the asymmetrical W 4f peaks (Figure 3c) showed the presence of a major doublet belonging to W(VI) from surface oxidation at 35.5 eV and a secondary, lower intensity doublet at 34.0 eV. The binding energies for W(V) and W(IV) are often close in value and it can be

difficult to precisely differentiate between the two states via XPS.[39] However, Xie et al have shown, through Ar+ bombardment studies on WO_3 nanowire films, the XPS peak fitting for various W states.[40] Their results show that W(V) and W(IV) appear at 34.3 (±0.2) and 33.2 (±0.2), respectively therefore suggesting that the secondary peaks observed in our CVD grown W:SnO_2 samples at 34.0 eV can be assigned to W(V).[40] A recent computational study by Fukumoto et al has also shown that +5 is most favorable oxidation state for W in W:SnO_2.[41]

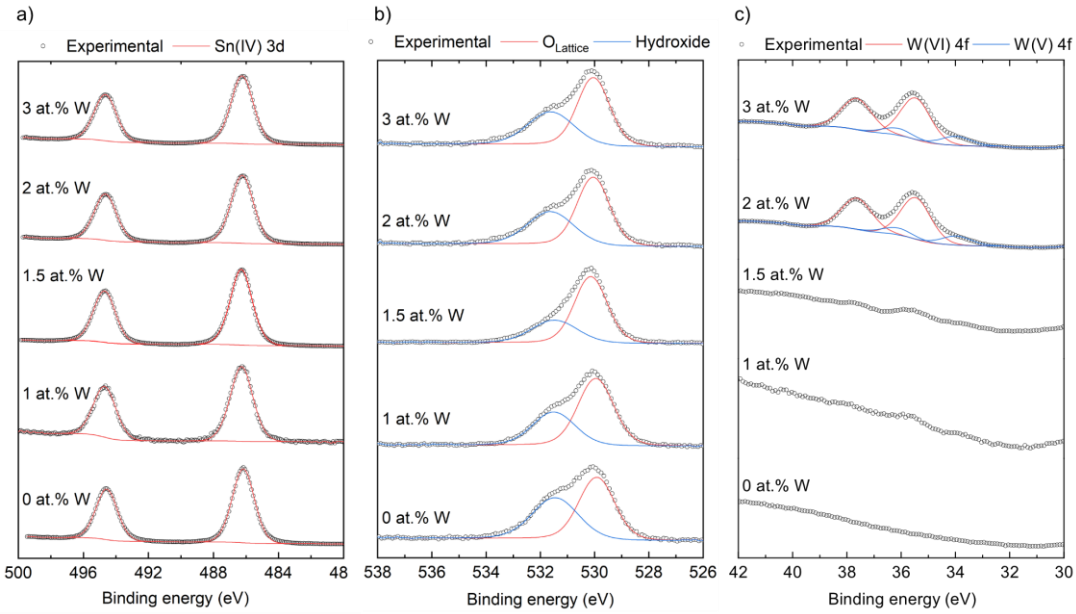

Figure 3: XPS results showing the a) Sn 3d, b) O 1s. and c) W 4f transitions for the W doped SnO_2 samples on glass. Sn was only found in the +4 oxidation state, oxygen bound to W in the lattice and in the form of surface OH groups were observed. W was present in both the +6 and +5 states in the higher doped samples.

The morphology and film thickness were measured using scanning electron microscopy (SEM) via a top down and side on set up (Figure 4 and ESI Figure S2, respectively). All films consist of compactly packed faceted grains often seen for SnO_2 and no significant change in morphology was observed upon W-doping. A similar compacted morphology was observed by Yu et al. for their W:SnO_2 films grown via magnetron sputtering and Kumar et al. observed densely packed nanosized domes for their chemical spray pyrolysis grown W:SnO_2 samples.[22,35] This morphology is typical for more established and commercially available SnO_2 TCO systems such as F:SnO_2 and Sb:SnO_2 that are used in, for example, PV devices, therefore highlighting the compatibility of the CVD grown W:SnO_2 films for such uses too.

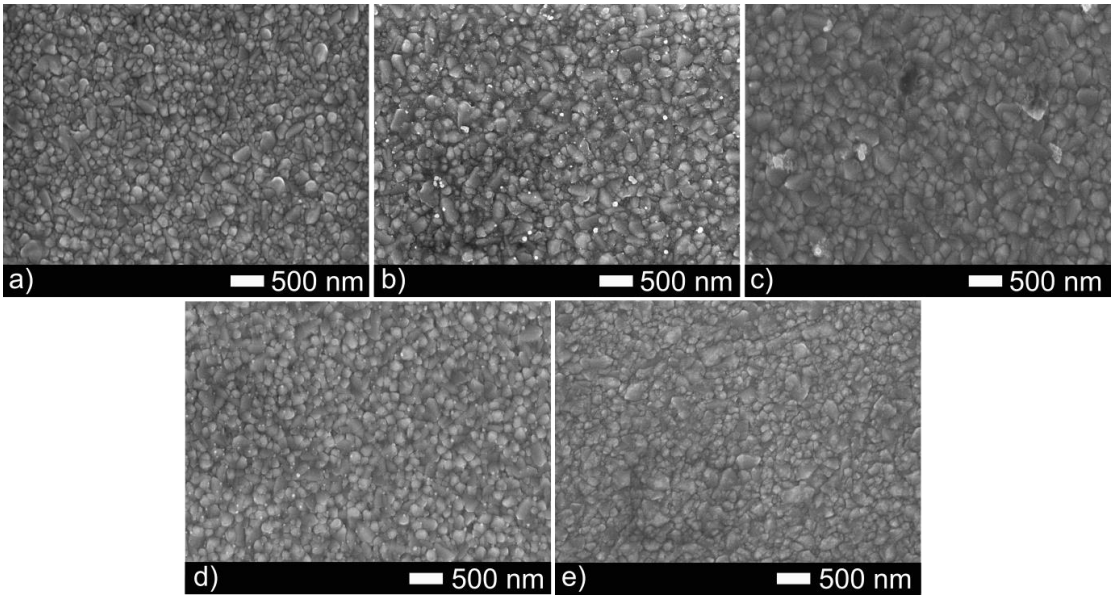

Figure 4: SEM images showing a faceted morphology for a) 0 at.%, b) 1 at.%, c) 1.5 at.%, d) 2 at.% and e) 3 at.% W doped SnO_2 films.

The optical measurements of the nominally undoped and W-doped SnO_2 films were obtained using an UV/visible/IR spectrometer (Figure 5a). All films had ~80% transmittance across the visible wavelengths apart from the highly doped samples where transmittance dropped to 75 and 72% for 2 and 3 at%, respectively. The transmittance of the films to light of 550 nm wavelength was high at 86, 82, 82% for the 0, 1 and 1.5 at.% , however lower values of 75 and 72% were obtained for the 2 and 3 at.% concentrations possibly due to increased light scattering from grain boundaries and secondary phases. Reflectance was also low at >20% in the visible however an increased reflectance to near-IR light (and concurrent decreased transmittance) was observed due to the screening effect of the carrier electrons in resonance with the incident NIR photons. With increasing carrier concentration, the plasmon edge is blue shifted (as shown in Table 2) and the optical window, as measured from the band gap to the plasmon edge, was reduced. For the 1.5 at.% doped sample, that had the highest carrier concentration of 3.66 x 10^{20} cm^{-3}, the plasmon edge was situated at 2312 nm which is still considerably higher than 1625 nm measured for ATO films with a carrier concentration of 3.6 x 10^{20} cm^{-3} that were grown via CVD.[42] Thus for instances where high transmittance across visible and IR wavelengths is advantageous, e.g. for electrodes in

tandem cell photovoltaics, the CVD grown W:SnO_2 films should allow for higher device efficiency.[43,44]

The band gap was derived from the UV-vis-NIR optical data by using the Poeppelmeier adaption of the Tauc method for polycrystalline degenerately doped semiconductors (Figure 5b).[45,46] Here, the difference between the x-intercepts of the tangents of $(\alpha h\nu)$ and $(\alpha h\nu)^2$ is added to the Tauc band gap to give the corrected band gap that accounts for the broadening of electron-hole pair states after optical absorption in crystalline materials.[46] Both the nominally undoped film and the W:SnO_2 films had a Tauc method band gap of 3.6 eV and a corrected band gap of 3.7 eV. The lack of any observable band gap shift to higher energies as a result of the Moss-Burstein effect is attributed to the relatively low carrier concentration (2.33 – 3.66 x 10^{20} cm^{-3} – Table 2) in the W:SnO_2 films.

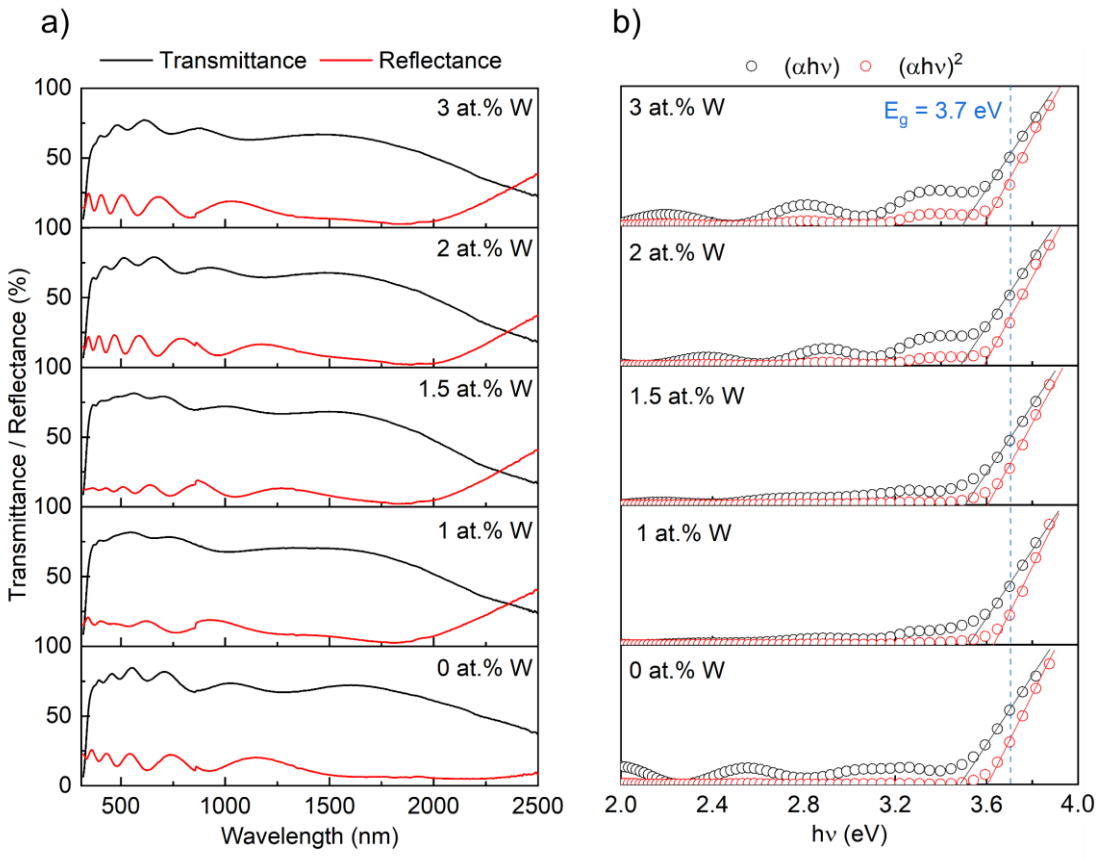

Figure 5: a) Transmittance and reflectance spectra doped SnO_2 films grown on barrier coated glass substrates. b) Corrected Tauc plots showing the optical band gap of the SnO_2 and W:SnO_2 thin films.

The electrical properties determined via Hall effect measurements are presented in Table 2. The nominally undoped SnO_2 film had a resistivity of $1.9x10^{-3}$ Ω.cm which is not abnormal for SnO_2 grown *via* AACVD using methanol as a solvent.[9,10,47] This intrinsic conductivity in SnO_2 is thought, from computational studies, to arise mainly from oxygen vacancies.[47,48] As W was introduced the carrier concentration increased from 1.1 x 10^{20} cm^{-3} for the undoped sample to 2.33 x 10^{20} cm^{-3}, then to a maximum of 3.66 x 10^{20} cm^{-3} before reducing slightly to 2.48 x 10^{20} cm^{-3} and 2.57 x 10^{20} cm^{-3} for the 1, 1.5, 2 and 3 at.%, respectively. This was due to successful replacement of Sn^{4+} in the SnO_2 matrix with W^{5+} resulting in the donation of one electron per substitution to enhance conductivity. At the higher W levels of 2 and 3 at.%, the carrier concentration was reduced, likely due to charge compensating species in SnO_2 such as the neutral impurity (W^{4+}) states and the formation of electrically insulating secondary phases.[41,47] This has previously been seen for W-doped SnO_2 films grown *via* other methods and in Sb-doped SnO_2 films.[16,18,35,47]

The optimal W concentration was found to be 1.5 at.% which yielded a resistivity of 5.9 x 10^{-4} Ω cm and a sheet resistance of 11.4 $\Omega.\square^{-1}$. This is comparable to commercially available FTO (see Table 1) and the lowest resistivity values reported for W:SnO_2 films on glass substrates (Figure 6).[49] The low resistivity achieved in this study is due to maximizing electron mobilities despite extrinsic doping and increasing carrier concentrations (Table 2). Similar to IMO and Ta:SnO_2 systems, this was due to: 1) minimal disturbance of the SnO_2 CBM by W states due to the W 5d band situated 1.39 eV above the CBM therefore allowing for low electron effective mass and 2) W^{5+} being the dominant dopant in SnO_2 therefore minimizing any ionized impurities scattering.[20]

In our CVD grown polycrystalline W:SnO_2 films, the carrier concentration values (2.33 – 3.66 x 10^{20} cm^{-3}) are low and comparable to those obtained by Nakao et al (2.4 $x10^{20}$ cm^{-3}) for W:SnO_2 on TiO_2 substrates via PLD.[18] At these low concentrations, grain boundary scattering of carriers can play an important role in limiting carrier mobility and resistivity – hence explaining the lower resistivity and mobility values observed for polycrystalline films grown on glass vs TiO_2 seed layers.[18]

Table 2: The carrier concentration (n), electron mobility (μ), resistivity (ρ) and sheet resistance (R_{sh}). The film thicknesses (d) determined via side-on SEM, average transmittance across the visible wavelengths and at 550 nm as well as the plasmon edge ($\lambda_{(plasmon)}$) are also listed. Values for commercially available NSG TEC™ 15 are also given.

W conc. / at.%	*d*/nm	*n*/ × 10^{20} cm^{-3}	μ/cm^2 V^{-1} s^{-1}	ρ/×10^{-3} Ω cm	R_{sh}/Ω □$^{-1}$	T $\lambda_{400-700\ nm}$	Tλ_{550}	$\lambda_{(plasmon)}$ /nm
0	500	1.10	29.6	1.92	38.3	80	86	--
1	500	2.33	33.9	0.79	15.8	80	82	2356
1.5	520	3.66	28.9	0.59	11.4	80	82	2312
2	500	2.48	29.7	0.85	17.0	75	75	2352
3	540	2.57	10.3	2.37	43.9	72	71	2368
Commercial standard								
TEC™ 15	350	4.4	29.7	0.47	13.4	--	--	--

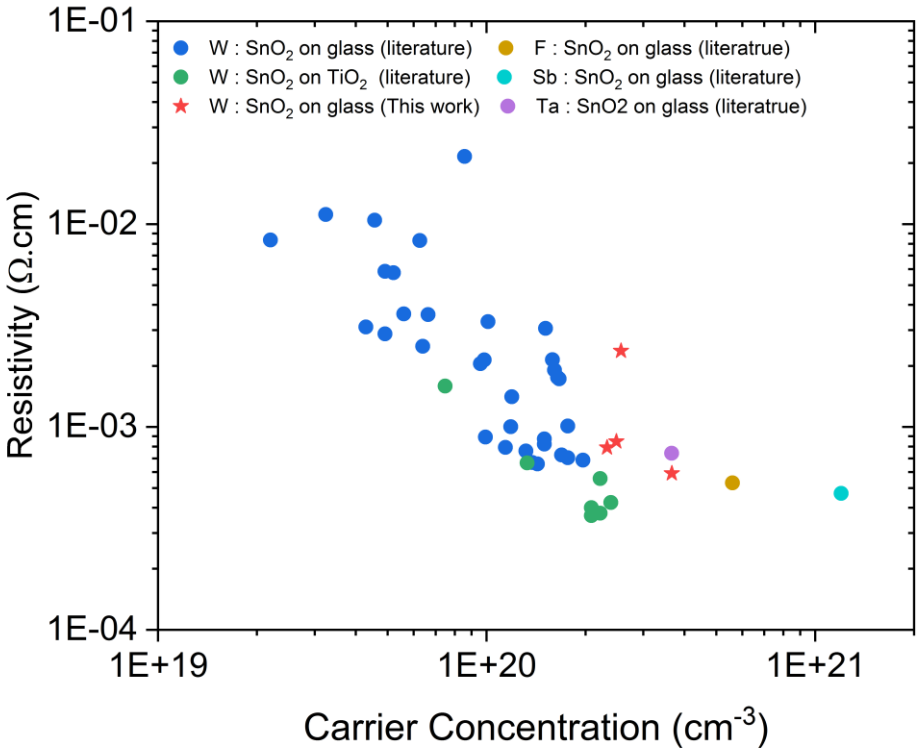

Figure 6: Plot resistivity vs carrier concentration for W : SnO_2 works found in the literature as well as this study based on CVD films.[15,18,21,35,50,51] **The plot also includes the**

electrical results of other popular SnO_2 based TCO systems such as F : SnO_2, Sb : SnO_2 and Ta : SnO_2 grown via CVD.[13,47,49]

Conclusion

The results presented in this paper show that resistivity as low as 5.9×10^{-4} Ω.cm for W:SnO_2 films are achievable using CVD under ambient pressure conditions on inexpensive glass substrates as opposed to pseudo epitaxial anatase TiO_2. Relatively high electron mobilities (~30 $cm^2V^{-1}s^{-1}$) were the main facilitator for the low resistivity and was achieved due to four favorable properties of W as a dopant for SnO_2.

1) W(V) 5*d* states are high in the conduction band of SnO_2 and cause minimal disturbance to the conduction band minima thus allowing low effective electron masses.

2) W induces crystallographic preferred orientation in the [200], the direction that is known to facilitate mobility.

3) The preference for W to occupy the +5 oxidation state in W:SnO_2, thus minimizing ionized impurity scattering.

5) Furthermore, W(V) is ideal as its ionic radius is closely matched to that of Sn(IV) therefore when substitutionally doped it causes minimal change to the SnO_2 unit cell.

Acknowledgements

S.S wishes to thank Dr Sebastian Dixon for helpful discussions and The School of Engineering, London South Bank University for S.P's PhD studentship.

Supporting Information

C 1s XPS, Side on SEMs

References

(1) Ginley, D. S.; Bright, C. Transparent Conducting Oxides. *MRS Bull* **2000**, *25* (8), 15–18.

(2) Dixon, S. C.; Scanlon, D. O.; Carmalt, C. J.; Parkin, I. P. N-Type Doped Transparent Conducting Binary Oxides: An Overview. *Journal of Materials Chemistry C*. Royal Society of Chemistry 2016, pp 6946–6961. https://doi.org/10.1039/c6tc01881e.

(3) Shi, J.; Zhang, J.; Yang, L.; Qu, M.; Qi, D.-C.; Zhang, K. H. L. Wide Bandgap Oxide Semiconductors: From Materials Physics to Optoelectronic Devices. *Advanced Materials* **2021**, 2006230.

(4) Heasley, R.; Davis, L. M.; Chua, D.; Chang, C. M.; Gordon, R. G. Vapor Deposition of Transparent, p-Type Cuprous Iodide via a Two-Step Conversion Process. *ACS Appl Energy Mater* **2018**, *1* (12), 6953–6963.

(5) Zhang, Y.; Liu, Z.; Ji, C.; Chen, X.; Hou, G.; Li, Y.; Zhou, X.; Cui, X.; Yang, X.; Ren, C. Low-Temperature Oxide/Metal/Oxide Multilayer Films as Highly Transparent Conductive Electrodes for Optoelectronic Devices. *ACS Appl Energy Mater* **2021**, *4* (7), 6553–6561.

(6) Minami, T. Transparent Conducting Oxide Semiconductors for Transparent Electrodes. *Semicond Sci Technol* **2005**, *20* (4), S35–S44. https://doi.org/10.1088/0268-1242/20/4/004.

(7) Ratnayake, S. P.; Ren, J.; Murdoch, B. J.; van Embden, J.; Gómez, D. E.; McConville, C. F.; della Gaspera, E. Nanostructured Electrodes Based on Two-Dimensional SnO2 for Photoelectrochemical Water Splitting. *ACS Appl Energy Mater* **2022**, *5* (9), 10359–10365.

(8) Lan, S.; Yoon, S.; Seok, H.-J.; Ha, H. U.; Kang, D.-W.; Kim, H.-K. Low-Temperature Deposited Highly Flexible In–Zn–V–O Transparent Conductive Electrode for Perovskite Solar Cells. *ACS Appl Energy Mater* **2021**, *5* (1), 234–248.

(9) Swallow, J. E. N.; Williamson, B. A. D.; Sathasivam, S.; Birkett, M.; Featherstone, T. J.; Murgatroyd, P. A. E.; Edwards, H. J.; Lebens-Higgins, Z. W.; Duncan, D. A.; Farnworth, M. Resonant Doping for High Mobility Transparent Conductors: The Case of Mo-Doped In 2 O 3. *Mater Horiz* **2020**, *7* (1), 236–243.

(10) Bhachu, D. S.; Scanlon, D. O.; Sankar, G.; Veal, T. D.; Egdell, R. G.; Cibin, G.; Dent, A. J.; Knapp, C. E.; Carmalt, C. J.; Parkin, I. P. Origin of High Mobility in Molybdenum-Doped Indium Oxide. *Chemistry of Materials* **2015**, *27* (8), 2788–2796. https://doi.org/10.1021/cm503896h.

(11) Ganose, A. M.; Scanlon, D. O. Band Gap and Work Function Tailoring of SnO 2 for Improved Transparent Conducting Ability in Photovoltaics. *J Mater Chem C Mater* **2016**, *4* (7), 1467–1475.

(12) Swallow, J. E. N.; Williamson, B. A. D.; Whittles, T. J.; Birkett, M.; Featherstone, T. J.; Peng, N.; Abbott, A.; Farnworth, M.; Cheetham, K. J.; Warren, P. Self-compensation in Transparent Conducting F-doped SnO2. *Adv Funct Mater* **2018**, *28* (4), 1701900.

(13) Williamson, B. A. D.; Featherstone, T. J.; Sathasivam, S. S.; Swallow, J. E. N.; Shiel, H.; Jones, L. A. H.; Smiles, M. J.; Regoutz, A.; Lee, T.-L.; Xia, X. Resonant Ta Doping for Enhanced Mobility in Transparent Conducting SnO2. *Chemistry of Materials* **2020**, *32* (5), 1964–1973.

(14) Kim, J.; Murdoch, B. J.; Partridge, J. G.; Xing, K.; Qi, D.; Lipton-Duffin, J.; McConville, C. F.; van Embden, J.; Gaspera, E. della. Ultrasonic Spray Pyrolysis of Antimony-Doped Tin Oxide Transparent Conductive Coatings. *Adv Mater Interfaces* **2020**, *7* (18), 2000655.

(15) Huang, Y.; Zhang, Q.; Li, G.; Yang, M. Tungsten-Doped Tin Oxide Thin Films Prepared by Pulsed Plasma Deposition. *Mater Charact* **2009**, *60* (5), 415–419.

(16) Wang, M.; Gao, Y.; Chen, Z.; Cao, C.; Zhou, J.; Dai, L.; Guo, X. Transparent and Conductive W-Doped SnO2 Thin Films Fabricated by an Aqueous Solution Process. *Thin Solid Films* **2013**, *544*, 419–426.

(17) Zhou, W.; Liu, L.; Yuan, M.; Song, Q.; Wu, P. Electronic and Optical Properties of W-Doped SnO2 from First-Principles Calculations. *Comput Mater Sci* **2012**, *54*, 109–114.

(18) Nakao, S.; Yamada, N.; Hitosugi, T.; Hirose, Y.; Shimada, T.; Hasegawa, T. Fabrication of Transparent Conductive W-doped SnO2 Thin Films on Glass Substrates Using Anatase TiO2 Seed Layers. *physica status solidi c* **2011**, *8* (2), 543–545.

(19) Shannon, R. D. t; Prewitt, C. T. Revised Values of Effective Ionic Radii. *Acta Crystallogr B* **1970**, *26* (7), 1046–1048.

(20) Fukumoto, M.; Hirose, Y.; Williamson, B. A. D.; Nakao, S.; Kimura, K.; Hayashi, K.; Sugisawa, Y.; Sekiba, D.; Scanlon, D. O.; Hasegawa, T. Ligand Field-Induced Exotic Dopant for Infrared Transparent Electrode: W in Rutile SnO2. *Adv Funct Mater* **2022**, *32* (14), 2110832.

(21) Huang, Y.; Li, D.; Feng, J.; Li, G.; Zhang, Q. Transparent Conductive Tungsten-Doped Tin Oxide Thin Films Synthesized by Sol–Gel Technique on Quartz Glass Substrates. *J Solgel Sci Technol* **2010**, *54* (3), 276–281.

(22) Kumar, M.; Kumar, A.; Abhyankar, A. C. Influence of Texture Coefficient on Surface Morphology and Sensing Properties of W-Doped Nanocrystalline Tin Oxide Thin Films. *ACS Appl Mater Interfaces* **2015**, *7* (6), 3571–3580.

(23) Marchand, P.; Hassan, I. A.; Parkin, I. P.; Carmalt, C. J. Aerosol-Assisted Delivery of Precursors for Chemical Vapour Deposition: Expanding the Scope of CVD for Materials Fabrication. *Dalton Trans* **2013**, *42* (26), 9406–9422. https://doi.org/10.1039/c3dt50607j.

(24) Sathasivam, S.; Arnepalli, R. R.; Kumar, B.; Singh, K. K.; Visser, R. J.; Blackman, C. S.; Carmalt, C. J. Solution Processing of GaAs Thin Films for Photovoltaic Applications. *Chemistry of Materials* **2014**, *26* (15), 4419–4424.

(25) Sathasivam, S.; Bhachu, D. S.; Lu, Y.; Chadwick, N.; Althabaiti, S. A.; Alyoubi, A. O.; Basahel, S. N.; Carmalt, C. J.; Parkin, I. P. Tungsten Doped TiO2 with Enhanced Photocatalytic and Optoelectrical Properties via Aerosol Assisted Chemical Vapor Deposition. *Sci Rep* **2015**, *5*.

(26) Sathasivam, S.; Williamson, B. A. D.; Kafizas, A.; Althabaiti, S. A.; Obaid, A. Y.; Basahel, S. N.; Scanlon, D. O.; Carmalt, C. J.; Parkin, I. P. Computational and Experimental Study of Ta<inf>2</Inf>O<inf>5</Inf> Thin Films. *Journal of Physical Chemistry C* **2017**, *121* (1). https://doi.org/10.1021/acs.jpcc.6b11073.

(27) Choy, K. L. Chemical Vapour Deposition of Coatings. *Prog Mater Sci* **2003**, *48* (2), 57–170.

(28) Cai, Z.; Liu, B.; Zou, X.; Cheng, H.-M. Chemical Vapor Deposition Growth and Applications of Two-Dimensional Materials and Their Heterostructures. *Chem Rev* **2018**, *118* (13), 6091–6133.

(29) Doebelin, N.; Kleeberg, R. Profex: A Graphical User Interface for the Rietveld Refinement Program BGMN. *J Appl Crystallogr* **2015**, *48* (5), 1573–1580.

(30) Mittal, K. L. Adhesion Measurement of Thin Films. *Electrocomponent science and technology* **1976**, *3* (1), 21–42.

(31) Krisyuk, V. v; Koretskaya, T. P.; Turgambaeva, A. E.; Trubin, S. v; Korolkov, I. v; Debieu, O.; Duguet, T.; Igumenov, I. K.; Vahlas, C. Thermal Decomposition of Tungsten Hexacarbonyl: CVD of W-containing Films under Pd Codeposition and VUV Assistance. *physica status solidi (c)* **2015**, *12* (7), 1047–1052.

(32) de Graaf, A.; van Deelen, J.; Poodt, P.; van Mol, T.; Spee, K.; Grob, F.; Kuypers, A. Development of Atmospheric Pressure CVD Processes for Highquality Transparent Conductive Oxides. *Energy Procedia* **2010**, *2* (1), 41–48.

(33) Jones, A. C.; Hitchman, M. L. *Chemical Vapour Deposition: Precursors, Processes and Applications*; Royal society of chemistry, 2009.

(34) Stöwe, K.; Weber, M. Niobium, Tantalum, and Tungsten Doped Tin Dioxides as Potential Support Materials for Fuel Cell Catalyst Applications. *Z Anorg Allg Chem* **2020**, *646* (18), 1470–1480.

(35) Yu, S.; Li, L.; Sun, Z.; Zheng, H.; Dong, H.; Xu, D.; Zhang, W. Characteristics of Transparent Conducting W-Doped SnO2 Thin Films Prepared by Using the Magnetron Sputtering Method. *Journal of the American Ceramic Society* **2015**, *98* (4), 1121–1127.

(36) Shannon, R. D. t; Prewitt, C. T. Revised Values of Effective Ionic Radii. *Acta Crystallogr B* **1970**, *26* (7), 1046–1048.

(37) Ghosh, R.; Basak, D.; Fujihara, S. Effect of Substrate-Induced Strain on the Structural, Electrical, and Optical Properties of Polycrystalline ZnO Thin Films. *J Appl Phys* **2004**, *96* (5), 2689–2692.

(38) Dupin, J.-C.; Gonbeau, D.; Vinatier, P.; Levasseur, A. Systematic XPS Studies of Metal Oxides, Hydroxides and Peroxides. *Physical Chemistry Chemical Physics* **2000**, *2* (6), 1319–1324.

(39) Khyzhun, O. Y. XPS, XES and XAS Studies of the Electronic Structure of Tungsten Oxides. *J Alloys Compd* **2000**, *305* (1), 1–6.

(40) Xie, F. Y.; Gong, L.; Liu, X.; Tao, Y. T.; Zhang, W. H.; Chen, S. H.; Meng, H.; Chen, J. XPS Studies on Surface Reduction of Tungsten Oxide Nanowire Film by Ar+ Bombardment. *J Electron Spectros Relat Phenomena* **2012**, *185* (3–4), 112–118.

(41) Fukumoto, M.; Hirose, Y.; Williamson, B. A. D.; Nakao, S.; Kimura, K.; Hayashi, K.; Sugisawa, Y.; Sekiba, D.; Scanlon, D. O.; Hasegawa, T. Ligand Field-Induced Exotic Dopant for Infrared Transparent Electrode: W in Rutile SnO2. *Adv Funct Mater* **2022**, 2110832.

(42) Ponja, S. D.; Williamson, B. A. D.; Sathasivam, S.; Scanlon, D. O.; Parkin, I. P.; Carmalt, C. J. Enhanced Electrical Properties of Antimony Doped Tin Oxide Thin Films Deposited: Via Aerosol Assisted Chemical Vapour Deposition. *J Mater Chem C Mater* **2018**, *6* (27). https://doi.org/10.1039/c8tc01929k.

(43) Yu, K. M.; Mayer, M. A.; Speaks, D. T.; He, H.; Zhao, R.; Hsu, L.; Mao, S. S.; Haller, E. E.; Walukiewicz, W. Ideal Transparent Conductors for Full Spectrum Photovoltaics. *J Appl Phys* **2012**, *111* (12), 123505.

(44) Ellmer, K. Past Achievements and Future Challenges in the Development of Optically Transparent Electrodes. *Nat Photonics* **2012**, *6* (12), 809–817.

(45) Tauc, J.; Grigorovici, R.; Vancu, A. Optical Properties and Electronic Structure of Amorphous Germanium. *physica status solidi (b)* **1966**, *15* (2), 627–637.

(46) Dolgonos, A.; Mason, T. O.; Poeppelmeier, K. R. Direct Optical Band Gap Measurement in Polycrystalline Semiconductors: A Critical Look at the Tauc Method. *J Solid State Chem* **2016**, *240*, 43–48.

(47) Ponja, S. D.; Williamson, B. A. D.; Sathasivam, S.; Scanlon, D. O.; Parkin, I. P.; Carmalt, C. J. Enhanced Electrical Properties of Antimony Doped Tin Oxide Thin Films Deposited via Aerosol Assisted Chemical Vapour Deposition. *J Mater Chem C Mater* **2018**, *6* (27), 7257–7266.

(48) Buckeridge, J.; Catlow, C. R. A.; Farrow, M. R.; Logsdail, A. J.; Scanlon, D. O.; Keal, T. W.; Sherwood, P.; Woodley, S. M.; Sokol, A. A.; Walsh, A. Deep vs Shallow Nature of Oxygen Vacancies and Consequent N-Type Carrier Concentrations in Transparent Conducting Oxides. *Phys Rev Mater* **2018**, *2* (5), 54604.

(49) Noor, N.; Parkin, I. P. Enhanced Transparent-Conducting Fluorine-Doped Tin Oxide Films Formed by Aerosol-Assisted Chemical Vapour Deposition. *J Mater Chem C Mater* **2013**, *1* (5), 984–996.

(50) Huang, Y.; Li, G.; Feng, J.; Zhang, Q. Investigation on Structural, Electrical and Optical Properties of Tungsten-Doped Tin Oxide Thin Films. *Thin Solid Films* **2010**, *518* (8), 1892–1896.

(51) Huang, Y.; Zhang, Q.; Li, G. Transparent Conductive Tungsten-Doped Tin Oxide Polycrystalline Films Prepared on Quartz Substrates. *Semicond Sci Technol* **2008**, *24* (1), 15003.

Table of contents figure